Spatial resolution of methods for measuring the light-emission profile in organic light-emitting diodes

AIP | Journal of Applied Physics

Spatial resolution of methods for measuring the light-emission profile in organic light-emitting diodes

M. Carvelli, R. A. J. Janssen, and R. Coehoorn

Citation: J. Appl. Phys. **110**, 084512 (2011); doi: 10.1063/1.3656443
View online: http://dx.doi.org/10.1063/1.3656443
View Table of Contents: http://jap.aip.org/resource/1/JAPIAU/v110/i8
Published by the American Institute of Physics.

Spatial resolution of methods for measuring the light-emission profile in organic light-emitting diodes

M. Carvelli,[1,a)] R. A. J. Janssen,[2] and R. Coehoorn[3]
[1]*Department of Applied Physics, Molecular Materials and Nanosystems, Eindhoven University of Technology, P.O. Box 513, 5600 MB Eindhoven, The Netherlands Philips Research Laboratories, High Tech Campus 4, 5656 AE Eindhoven, The Netherlands and Dutch Polymer Institute (DPI), P.O. Box 902, 5600 AX Eindhoven, The Netherlands*
[2]*Department of Applied Physics, Molecular Materials and Nanosystems, Eindhoven University of Technology, P.O. Box 513, 5600 MB Eindhoven, The Netherlands*
[3]*Department of Applied Physics, Molecular Materials and Nanosystems, Eindhoven University of Technology, P.O. Box 513, 5600 MB Eindhoven, The Netherlands and Philips Research Laboratories, High Tech Campus 4, 5656 AE Eindhoven, The Netherlands*

(Received 27 May 2011; accepted 31 August 2011; published online 26 October 2011)

An analysis is presented of the resolution limits of two alternative methods for deducing the light-emission profile in organic light-emitting diodes (OLEDs) from the angular and polarization dependent emission spectra. The comparison includes the "fit-profile" (FP) method, within which the known physics of the recombination process is employed to describe the shape of the profile using a strongly reduced number of degrees of freedom, and the Tikhonov method, which provides a more general solution. First, the cases of a delta-function shaped emission profile and a broad single-peak emission profile are investigated. It is demonstrated that for these cases a ~1 nm resolution of the peak position may be obtained, provided that the peak is positioned optimally in the OLED microcavity. Subsequently, an analysis is given for a double-peak emission profile and for a rectangular profile, as may be obtained in multilayer OLEDs, revealing a resolution of ~10 nm for the cases studied. It is suggested that, in general, an optimal analysis should be based on a combined Tikhonov-FP approach.
 [doi:10.1063/1.3656443]

I. INTRODUCTION

In the past five years, organic light-emitting diodes (OLEDs) have emerged as a promising option for energy-efficient solid-state lighting and for cheap light sources produced on flexible foils.[1] The luminous efficacies, of more than 100 lm/W to date[2] when using macroextractors for enhancing the light-outcoupling and 64 lm/W without macroextractors,[3] are obtained using multilayer structures of evaporation-deposited small-molecule organic semiconductors. Flexible OLEDs are usually based on a single active layer deposited by spin-coating or ink-jet printing. Within both technologies, a key factor that needs to be measured and controlled is the shape of the emission profile, i.e., the spatial distribution of the emitting excitons across the active layer thickness. Being able to accurately measure the emission profile makes it possible to better understand the voltage dependence of the light-outcoupling efficiency and (in multilayer OLEDs with closely spaced emissive layers) the color stability. Nanometer-scale resolution is required in order to investigate state-of-the-art devices, containing ~10–20 nm thick emitting layers.[2] The possibility to extract emission profiles with a high accuracy would also be essential to investigate the validity of recombination models.[4] We note that recently refinements of the standard Langevin-model have been proposed, by more properly including the Coulomb interactions between holes and electrons[5] and the effect of recombination with trapped charges.[6,7] Furthermore, being able to resolve a shift of the light emission profile during the device operational lifetime would provide valuable insight into degradation processes.

A fully experimental method for locating the emission zone, based on the addition of a small concentration of dye-molecules with a red-shifted emission to the emissive layer, has been introduced and applied successfully by Tang and co-workers.[8] However, the use of this "sense layer" method requires the fabrication of a series of additional OLEDs and its applicability depends on the availability of suitable dye molecules. The light-emission profile can also be obtained from an analysis of measured spectral intensities.[9–18,20] We recently proposed a comprehensive novel approach to solve this "inverse outcoupling problem."[20] Crucial elements are (i) the use of the full angular and polarization dependent emission spectra, extracted using a glass hemisphere, (ii) the use of a combined classical and quantum-mechanical microcavity model for properly treating the radiative decay probability and light-outcoupling efficiency, and (iii) the use of a flexible and problem-specific fit function describing the profile. Within this "fit-profile" (FP) approach, enhanced accuracy was obtained by describing the profile in a manner which is consistent with the physics of the known recombination process for the single-layer OLEDs studied. We note that also in earlier studies FP-approaches were employed, using more strongly constrained functions such as a parameterized exponential[10,15] or a double-exponential fit-profile function.[12] In some cases a single oscillating dipole was

a)Electronic mail: marco.carvelli@philips.com.

used to replicate the experimental data.[13] A different approach, allowing more flexibility in the profile shape, involves the use of a dense set of dipoles distributed uniformly across the emitting layer.[17–19] In Refs. 18 and 19, the contribution of the ensemble of dipoles is regularized, leading to a more smooth light emission profile. In all these earlier studies no analysis was given of the accuracy with which the experimental data were collected.

The resolution with which the light-emission profile may be reconstructed from, realistically, noisy spectral data was for the first time discussed in Ref. 20 for the case of a broad emission profile in a single-layer OLED. The analysis focused on the emitting layer thickness dependence of the resolution. A formal condition number analysis was performed, as well as a more practical study of the profiles as obtained from a large ensemble of spectral datasets created by adding random noise to the ideal noise-free dataset for the system studied. In this paper, we compare the resolution limits as obtained using FP-methods and as obtained using a well-established more general and (potentially) high-resolution inverse-problem solving approach, the Tikhonov-method,[21–23] using the same microcavity model and experimental data and employing the "ensemble method" mentioned above. Four specific cases are studied, relevant to single-layer, double-layer, and multilayer OLEDs. Depending on the case studied, the resolution limit is found to be in the range of ~1 to ~10 nm. We investigate the resolution as a function of the exciton position within the device, and show how one may design the device for optimal resolution. From the analysis, it is argued that the most optimal approach would be to use the FP-method employing a shape of the profile which is suggested by a pre-analysis using the Tikhonov method.

In Sec. II, the FP-method and the Tikhonov method, as applied to the inverse light-outcoupling problem, will be described. In Sec. III, a comparison is given between the two methods for the four specific cases studied. A summary and conclusions are given in Sec. IV. In Appendix an analysis is given of the experimental precision and accuracy.

II. THEORETICAL METHODS

The FP and Tikhonov methods involve both a least-squares minimization of a weighed difference between the experimental spectra, measured as a function of the angle and the polarization, and modeled emission spectra. Both experimental and modeled spectra are normalized over the sum of the intensities, in order to enhance the sensitivity to the lower-intensity tails of the spectrum.[20] This also makes it possible to extract the "source spectrum," as will be shown later in this section and as was already discussed in Ref. 20. The calculated emission spectra derive from incoherently oscillating dipoles. The OLED stack is modeled as an optical microcavity, using a computer simulation tool, Lightex, developed at Philips Research Aachen.[24] The simulations include optical absorption in the emitting layer ("self-absorption"), optical anisotropy and the microcavity effect on the ratio of the radiative and non-radiative decay rates, as described in Ref. 20. In all cases, the emission is considered from a source spectrum with a uniform intensity in the 450 to 600 nm wavelength (λ) range, as probed in $M = 31$ equidistant wavelength steps and in $N = 36$ equidistant polar angles (θ) steps in the 0° to 70° range, and for s and p polarization. The intensities can be expressed as an experimental vector b of length $2M \times N$. The profile to be determined is expressed by a (dense) set of weights of discrete dipoles at equidistant points across the OLED, given by the vector x. Solving the inverse outcoupling problem then implies finding the solution of the equation $A \cdot x = b$, where A is the matrix which models the emission from the OLED microcavity.

Within the FP-method, the dipole weights at each of the grid points are constrained to a specific form of the emission profile, described by only a small number of free parameters. These are obtained by minimizing the difference between the emission intensity as predicted from these parameters and the experimental emission intensities, using a least-squares fitting routine. The parameterization of the fit profile will be adapted optimally to the problem to be solved, as explained in more detail in the case studies given in section III. By making use of a fit profile the reconstructed profile can be constrained to a physically realistic form, with intensities which are non-negative everywhere, zero at the electrode interfaces in the case of injection under thermal equilibrium conditions, and a restricted number of minima and maxima. In order to make this paper sufficiently self-contained, we briefly summarize the procedure applied to determine the light emission profile, reported in Ref. 20. As a first step, the experimental s and p polarized emission intensities $I^{\mathrm{expt}}_{s(p)}(\lambda,\theta)$ are normalized using the expression

$$I^{\exp t}_{\mathrm{norm},s(p)}(\lambda,\theta) = \frac{I^{\exp t}_{s(p)}(\lambda,\theta)}{S^{\exp t}_{s(p)}(\lambda)}, \tag{1}$$

with

$$S^{\exp t}_{s(p)}(\lambda) \equiv \frac{1}{N}\sum_{j=1}^{N} I^{\exp t}_{s(p)}(\lambda,\theta_j) \tag{2}$$

angle-averaged experimental spectral intensities. In the same manner, the normalized s and p emission spectra for a trial emission profile $P(\delta)$, where δ is the normalized distance to the anode, and a trial dipole orientation θ_d are calculated, making use of the emission $I^{\mathrm{calc}}_{s(p)}(\lambda, \theta, \delta, \theta_{\mathrm{d}})$ from unit dipoles at a position δ obtained from the Lightex program

$$I^{\mathrm{calc,trial}}_{\mathrm{norm},s(p)}(\lambda,\theta) = \frac{\int_0^1 P(\delta) I^{\mathrm{calc}}_{s(p)}(\lambda,\theta,\delta,\theta_d)d\delta}{S^{\mathrm{calc,trial}}_{s(p)}(\lambda)}, \tag{3}$$

with

$$S^{\mathrm{calc,trial}}_{s(p)}(\lambda) \equiv \frac{1}{N}\sum_{j=1}^{N}\int_0^1 P(\delta) I^{\mathrm{calc}}_{s(p)}(\lambda,\theta_j,\delta,\theta_d)d\delta \tag{4}$$

angle-averaged calculated spectral intensities. The starting point of the calculation is thus a flat emission spectrum. The

optimal emission profile and dipole orientation are found by minimizing the quantity

$$\chi^2 \equiv \sum_{i=1}^{M}\sum_{j=1}^{N}\sum_{s,p}\left\{I^{\mathrm{calc,trial}}_{\mathrm{norm},s(p)}(\lambda_i,\theta_j) - I^{\mathrm{exp}\,t}_{\mathrm{norm},s(p)}(\lambda_i,\theta_j)\right\}^2. \quad (5)$$

From the angle-averaged spectral intensities obtained for the optimized parameter set the source spectrum is then calculated using

$$S_{\mathrm{source}}(\lambda) = \frac{S_s^{\mathrm{expt}}(\lambda) + S_p^{\mathrm{expt}}(\lambda)}{S_s^{\mathrm{calc,opt}}(\lambda) + S_p^{\mathrm{calc,opt}}(\lambda)}. \quad (6)$$

The fit-profile method makes it possible to include constraints which lead to a solution which is consistent with assumptions made concerning the transport and recombination physics. However, it is not always *a priori* clear which assumptions would be most appropriate. In such cases, sufficient freedom should be given to the shape of the solution. The most general approach would be an unconstrained χ^2-method, within which the dipole weights at a dense set of grid points across the full thickness of the emissive layer are the degrees of freedom. For solving the corresponding inverse problem, we have used numerical methods which are standardly available,[25] including a non-negativity constraint which is obviously required to obtain physically realistic profiles. We will indicate this approach as the "non-negativity-constrained (NNC) χ^2-method."

Although non-negativity constrained solutions are already much more realistic than unconstrained solutions, it is often found that the problem is still to such an extent ill-posed that large unphysical point-to-point variations in the dipole intensities are obtained. An often-used method which makes it possible to reduce such variations is the Tikhonov-method.[21–23] Within this method, the quantity $\|A\cdot x - b\|^2 + \alpha^2\|x\|^2$ is minimized. Here the symbol $\|\|$ refers to the 2-norm of the vector and α is a parameter which controls the weight given to a penalty term $\alpha^2\|x\|^2$. We have employed this "regularization" method, again including a non-negativity constraint. In the $\alpha = 0$ limit, the Tikhonov method thus reduces to the non-negativity-constrained χ^2-method. Although the dipole weights can still have any positive value, strong variations are damped by the inclusion of the penalty term. This is known as the zeroth-order Tikhonov approach. Higher (nth) order approaches have been defined, by substituting $\|x\|$ with the 2-norm of the nth-order derivative of x. However, we restrict the discussion here to the zeroth-order approach. In practice, a trade-off will arise between the minimization of $\|A\cdot x - b\|^2$ and of $\|x\|^2$. The optimum value of α is then often chosen as the value at the corner of the L-shaped curve connecting the optimal $\{\|A\cdot x - b\|^2,\ \|x\|^2\}$ points as calculated as a function of α. The corner is defined as the point of maximum curvature of this curve. This is known as the "L-curve criterion."[23] An example of this approach will be given below (Fig. 3). The optimization procedure used within the Tikhonov method is similar to the one described by Eqs. 1–4 and 6, but the χ^2 error is given by

$$\chi^2 \equiv \sum_{i=1}^{M}\sum_{j=1}^{N}\sum_{s,p}\left\{I^{\mathrm{calc,trial}}_{\mathrm{norm},s(p)}(\lambda_i,\theta_j) - I^{\mathrm{exp}\,t}_{\mathrm{norm},s(p)}(\lambda_i,\theta_j)\right\}^2 + \alpha^2\sum_{k=1}^{Q}(x_k)^2, \quad (7)$$

where Q is the total number of dipoles considered. A grid point distance of 1 nm is used throughout this paper, with the first and last grid points at 8 nm distance from the electrodes.

The dipole intensities x_k are normalized such that their sum is equal to 1.

III. SPATIAL RESOLUTION—FOUR CASE STUDIES

In this section, we analyze the spatial resolution with which the emission profile can be determined for four cases, schematically represented in Fig. 1. In all cases, a 160 nm thick emissive layer is present in between glass/ITO/PEDOT:PSS (anode) and Ba/Al (cathode) layers, with the same layer thicknesses and refractive index functions as used in the previous section (and taken from Ref. 20). The figure gives the profile distributions as a function of the distance from the PEDOT:PSS/(emitting layer) interface. The first case (a) deals with emission from a delta-function shaped profile, i.e., an infinitely narrow zone located at a distance z_1 from the anode. In the second case (b) a single-peaked, broad emission profile similar to those deduced earlier from the analysis of blue polymer OLEDs (Refs. 20 and 26) are analyzed. Case (c) deals with the emission from multiple regions, described as two delta-like profiles located at a distance z_1 and z_2 from the anode. Case (d) considers the possibility to have a uniform emission profile over a narrow region. The last two profile shapes could be generated, for example, at the organic-organic interface in multilayer devices (c) or in between interfaces (d). In all cases an ensemble of 100 artificial "experimental datasets" (b-vector, see Sec. II) is created by adding Gaussian noise to the calculated emission spectra. Following the experimental precision and

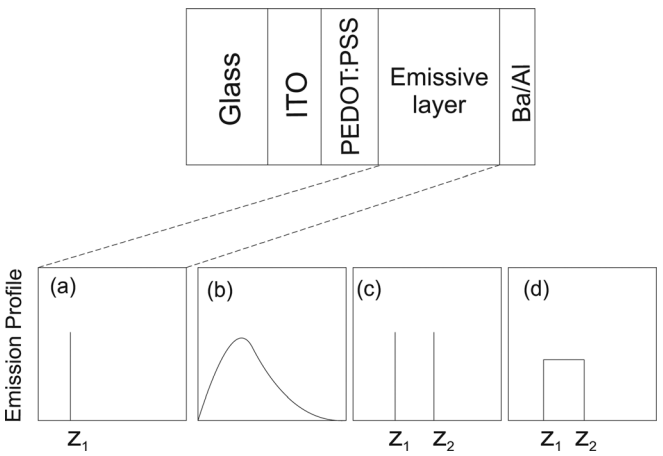

FIG. 1. Schematic representation of the four emission profile cases analyzed. (a) Delta-function shaped emission profile, located at a distance z_1 from the anode. (b) Broad single-peaked emission profile as obtained for a realistic device.[20,26] (c) Double delta-function shaped emission profile, with peaks at a distance z_1 and z_2 from the anode. (d) Rectangular emission profile, located in the range z_1-z_2 from the anode.

accuracy analysis given in the Appendix, 2% random noise is used for case (b), and 5% random noise is used for the other cases. In the Appendix, it is also shown how the experimental conditions are optimized in order to avoid or drastically reduce systematic errors. In each case, the FP and the Tikhonov methods are applied to the complete ensemble of artificial experimental data, in order to be able to determine the resolution with which the light-emission profile can be reconstructed.

A. Emission at one interface: delta-function shaped profile

In order to study the ultimate achievable resolution we consider as a first case the emission from a single dipole position in the emissive layer, i.e., from a delta-function shaped emission profile. Such a profile can arise in a bilayer OLED due to emission from charge-transfer excitons which are confined to the interface, when the electron and hole transport layers are at the same time hole and electron blocking, respectively.

First, we have analyzed the accuracy with which the profile can be reconstructed using the fit profile method, assuming a Gaussian profile with a peak shift Δ [as defined in the inset of Fig. 2(a)] and the peak width as free parameters. Figure 2(a) (full spheres) shows the ensemble-averaged value of the peak shift (error) Δ as a function of the distance to the anode. The gray regions give the 99.6% confidence interval on the peak position error. A positive error corresponds to a peak position further from the anode as compared to the real peak position. It is found that in all cases the error is of the order of 1 nm, and smallest at a distance of 120 nm from the cathode (40 nm from the anode). For dipoles located close to the cathode the error gets larger, although the uncertainty is still always less than 3 nm. For dipoles more close to the anode, the error increases only slightly. An otherwise identical calculation for a 320 nm device revealed the same position dependence of the error in the peak position and uncertainty interval in the region within 120 nm from the cathode. The error and its uncertainty were found to stay significantly smaller than 1 nm for larger distances from the cathode.

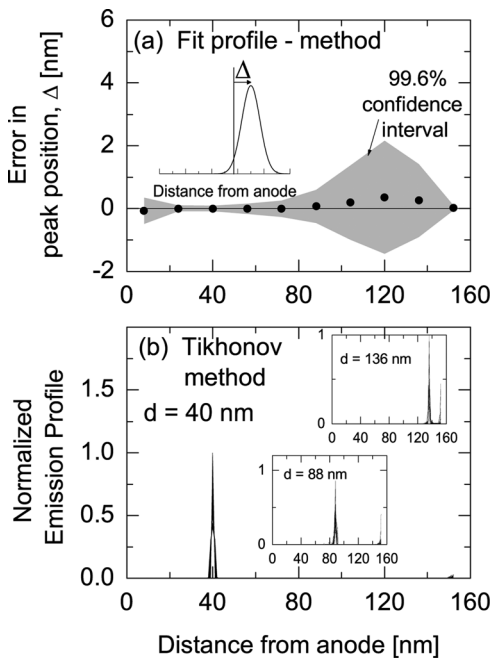

FIG. 2. Single-delta profile resolution. (a) Fit-profile method results. Error in the peak position determination, Δ, defined as in the inset, as a function of the distance of the emitting plane from the anode. The full dots indicate the average over 100 noise configurations, while the gray region describes a 99.6% confidence interval. (b) Tikhonov-method results, with $\alpha = 0$, for emission at three different distances (d) from the anode.

Figure 2(b) describes the results obtained using the Tikhonov method with $\alpha = 0$. The method reduces in this case to a non-negativity constrained χ^2-method. No regularization is used, as that would immediately widen the profile. As noted above, the analysis was done for a discrete set of dipole positions at a 1 nm mutual distance. The determined emission profiles obtained for emission at three different distances from the anode are given. The peak position is in all cases retrieved within 1 nm, and the width of the profile is almost equal to the 1 nm distance between the dipole positions used. The resolution is thus in this case essentially as good as that of the FP-method. However, it may be noted that artifacts in the form of additional peaks are present very close to the cathode. Their weight increases if the actual emission position approaches the cathode [see Fig. 2(b)]. This intensity may be explained as a result of the very small outcoupling efficiency for emission from a position close to the cathode, so that the χ^2 function is almost insensitive to spurious high dipole intensities near the cathode.

B. Broad emission profile

In single-emissive-layer devices, a broad and single-peaked emission profile is expected, as observed, e.g., for the case of blue and red emitting polymer OLEDs[20] and as predicted from drift-diffusion-recombination modeling.[4,26,27] In this subsection, the ensemble of artificial data is based on the emission profile for a 160 nm thick blue-emitting OLED, driven at 18 V, as obtained in the framework of the study presented Ref. 26. Figure 4(f) of that paper shows the voltage dependence of the emission profile deduced. The profile was described in terms of its peak position, peak width and peak asymmetry in a manner described in Ref. 20. The same three-parameter approach is also used in this paper when employing the FP-method. The emission profiles obtained using the FP and Tikhonov methods are given in Figs. 3(a) and 3(b–d), respectively.

Figure 3(a) shows that the ensemble of 100 reconstructed profiles as obtained from the FP method reveals that the uncertainty resulting from the 2% random noise included is very small. The original profile (not shown) coincides with the average of the curves displayed. The original profile can thus be reconstructed with nanometer-scale resolution, as concluded already in Ref. 20. In Fig. 3(b), the results for the Tikhonov method with a relatively small regularization parameter ($0.03 \times \alpha_{corner}$ are presented, and Figs. 3(c) and 3(d) show the results obtained using the Tikhonov approach using $\alpha = 0$ and $\alpha = \alpha_{corner}$, i.e., at the corner point of the L-curve, shown in Fig. 3(e). In the absence of regularization [Fig. 3(c)], the resulting profiles show huge point-to-point

variations, unlike the smooth original profile (white curve). A non-zero value of α, but still smaller than the corner-point value [Fig. 3(b)], gives rise to an ensemble of profiles which describe, on average, the original profile. However, additional intensity arises near the cathode, an artifact which was already visible for the $\alpha = 0$ case and which was also found for emission from a delta-function profile in the previous subsection. When α is equal to the corner-point value [Fig. 3(d)], the point-to-point variations have essentially vanished. However, the original profile (dashed) is not correctly retrieved. It is too wide near the peak, and the reconstruction shows an even more strong intensity near the cathode than as obtained using less regularization.

We conclude that it is within the Tikhonov method not trivial to choose the most appropriate value of the optimization parameter. The non-regularized profiles are very noisy and provide little information about the original profile, showing (at best) that the emission originates from a region more close to the anode, whereas the profiles obtained for α_{corner} produce a strong artifact close to the cathode. The use of an α value in between zero and the corner point seems in this case to be preferable, provided that a large ensemble of nominally identical experimental data sets would be available. The analysis shows that even without such an additional effort the FP method already gives rise to a very accurate reconstructed profile.

C. Emission at two interfaces

In efficient multilayer OLEDs, the recombination and emission takes place in a central layer, sandwiched in between hole transporting and electron transporting layers which are blocking for electrons and holes, respectively. In the case of well-balanced electron and hole mobilities, charge accumulation at the two internal interfaces can give rise to recombination which is strongly localized at these interfaces. We investigate here to what extent the emission from the two interfaces can be resolved experimentally. For that purpose, we consider a double delta-function shaped emission profile from two positions in the 160 nm thick emissive layer, viz., from a first interface at 24 nm from the anode, and from a second interface at 40, 56, or 72 nm from the anode. We consider thus emission from the region in the OLED for which from the analysis given in Sec. III A the highest resolution is expected. Equal intensities for the emission from both interfaces are assumed. The three cases have been studied using the FP-approach and using the Tikhonov approach with $\alpha = 0$. The results are given in Figs. 4(a)–4(c) and 4(d)–4(f), respectively, which in all cases show a superposition of all reconstructed profiles as obtained for an ensemble of 100 artificial datasets.

Using the FP-approach, the presence of the two separate peaks can be retrieved when their distance is 24 nm or larger [Figs. 4(a) and 4(b)]. When their distance is 16 nm [case (c)], the spread in the peak distribution is so large that the two peaks cannot be distinguished anymore. Using the Tikhonov-method it is in all cases possible to resolve the presence of two distinct peaks, even at a distance as small as 16 nm, although in this case the profiles obtained start to show additional smaller peaks in the region in between the two interfaces and although (as observed also above) additional intensity is found close to the cathode.

We conclude that for this case the ultimate resolution is not as good as would be expected from the resolution obtained for the case of a single delta-function shaped profile studied in Sec. III A, and that the Tikhonov approach shows in this case a somewhat better resolution.

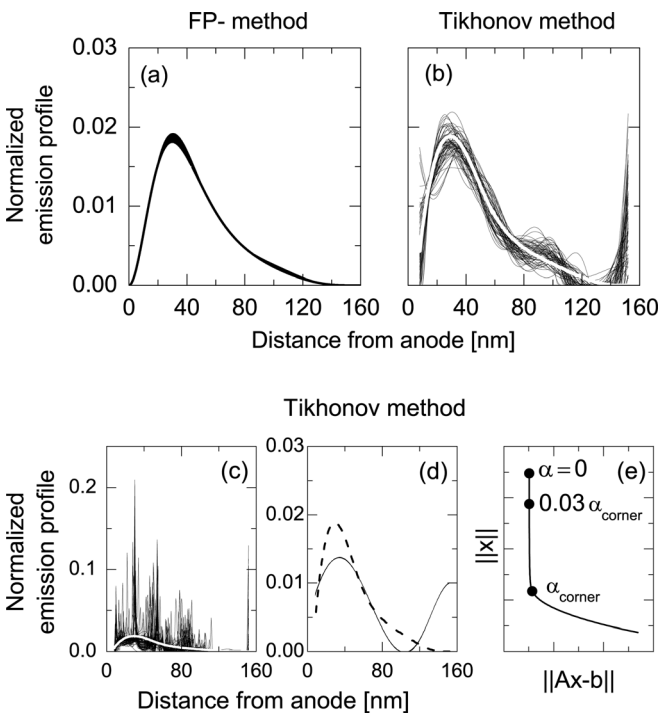

FIG. 3. Reconstructed emission profiles for a broad single-peaked profile case, for a profile determined for a 160 nm thick blue-emitting OLED, driven at 18 V, as obtained using the FP-method (a) and as obtained using the Tikhonov method with regularization parameter $\alpha = 0.03 \cdot \alpha_{corner}$ (b), $\alpha = 0$ (c), and $\alpha = \alpha_{corner}$ (d), with α_{corner} as deduced from the L-curve (e). The original profile coincides with the average of the profiles shown (a), is given in white (b,c) or is given as a dashed curve (d).

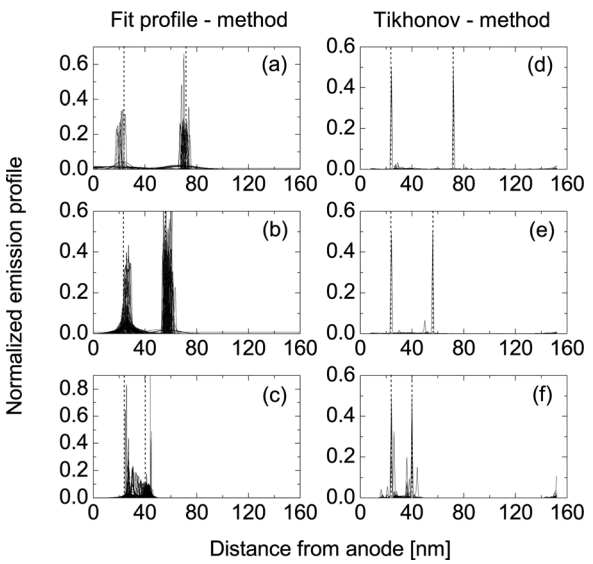

FIG. 4. Light-emission profiles as determined using the FP (a–c) and Tikhonov (d–f) approaches for emission at a distance of 24 nm (fixed) and 72 (a,d), 56 (b,e), and 40 nm (c,f) from the anode, indicated by dashed lines.

D. Uniform emission in between two interfaces: rectangular profile

In multilayer OLEDs such as considered in the previous subsection, the emission from the central emissive layer can also be uniform. The emission profile is then rectangular. It may be shown from drift-diffusion-recombination device modeling that such a situation arises if the mobility in the transport layers is much larger than the mobility (for both carriers) in the emissive layer, if the mobility is constant and equal for electrons and holes, and if charge-carrier diffusion may be neglected. Designing OLEDs such that the emission originates from the entire emissive layer, instead of from the interface regions, is expected to give rise to an enhanced operational lifetime. It is therefore of interest to be able to distinguish experimentally emission from the rectangular profile assumed from emission originating from the two interface regions. We consider uniform emission from a range 36 to 44 nm from the anode.

Within the fit-profile analysis we try to reconstruct the profile by describing it as a superposition of a rectangular profile and two delta-function peaks [see Fig. 5(a)]. All 100 artificial datasets were found to lead, within 1 nm, to the correct original value of the boundary positions of the profile. Furthermore, the weight (w_3) given to the rectangular component was found to be on average very large, viz., $87 \pm 11\%$, and the average weights of the two delta-function peaks at the interfaces (w_1 and w_2) were almost equal and quite small, as shown in the figure. The FP-approach is thus able to provide a quite accurate picture of the recombination process, being distributed uniformly over the emissive layer instead of being peaked at the interfaces.

Analyzing the same ensemble of 100 artificial datasets with the Tikhonov approach, the results shown in Fig. 5(b) are obtained. The original profile is here represented in white, while the ensemble of reconstructed profiles as obtained without regularization ($\alpha = 0$) is shown in black. It is found that the width and the position of the rectangle are correctly retrieved. The reconstructed emission zone coincides almost completely with the original 36–44 nm emission zone. However, the uniformity of the emission is not retrieved. Instead, a rather noisy profile is in all cases obtained. Furthermore, also (again) some intensity is found near the cathode (not shown). In gray, we give for a specific dataset the L-curve corner profile; the other datasets yield almost identical profiles. Regularizing the solution thus smoothes the curve, however at the expense of a loss of sharpness in the profile.

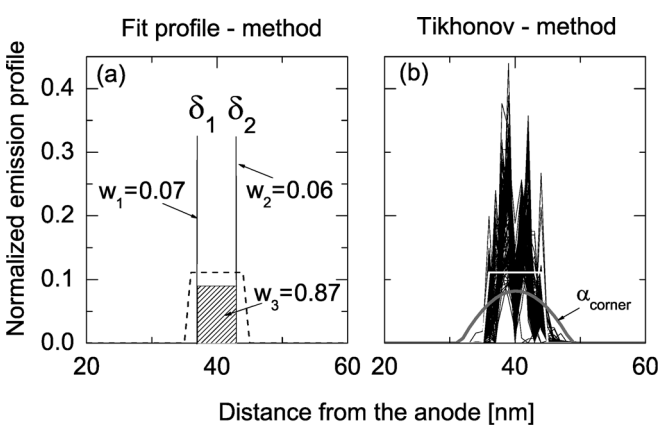

FIG. 5. Reconstruction of a rectangular light-emission profile. (a) Results of the fit-profile method, indicating the average weights w_1 and w_2 obtained for the two assumed delta-function emission peaks at the interval edges and the average weight w_3 for the uniform emission profile. The edge positions are $\delta_1 = 36$ and $\delta_2 = 44$ nm are almost perfectly retrieved. Original profile: dashed curve. (b) Results of the Tikhonov method, indicating in black the ensemble of profiles obtained without regularization ($\alpha = 0$), and in gray a single profile obtained after regularization using L-curve corner point α_{corner}. Original profile: white curve.

IV. CONCLUSIONS

The resolution limits of two inverse-problem solving approaches for reconstructing the light-emission profile from experimentally collected electroluminescence spectra in OLEDs were investigated. The FP method is based on a parameterized emission profile, while the Tikhonov method produces profiles free of any assumption concerning the shape. The only constraint is the non-negativity of the solution. Both methods have been applied to four cases: a delta-function shaped profile as may be obtained for a bilayer OLED, a broad single-peak profile as may be obtained for a single-layer OLED, a double delta-function shaped profile and a rectangular profile as may be obtained for a multilayer OLED. In Appendix an analysis of the experimental precision and accuracy is given.

In the two narrow emission profile cases studied (single and double delta-function peak shaped profiles) we have found nanometer-scale resolution of the peak positions for both approaches, with the non-regularized Tikhonov method ($\alpha = 0$) leading to a better resolution for the double-delta-function shaped profile. In the two broad emission profile cases studied (broad single-peak profile and rectangular profile) we have found that the FP-approach provides accurate reconstructions with nanometer-scale resolution. In such cases the Tikhonov approach quite accurately provides unbiased information about the region in the device from which the emission predominantly originates. However, the profiles obtained show strong point-to-point intensity variations which can only be damped out by means of regularization at the expense of a loss of sharpness or resolution. Furthermore, in all four cases the Tikhonov method gives rise to intensity artifacts near the cathode, in particular when using strong regularization. We note that the resolution limits given were based on conservatively chosen experimental noise levels, and that the development of lower-noise measurement techniques could give rise to further improved resolution.

For the case of relatively wide emission profiles for which the shape is not *a priori* known, our analysis suggests that an improved method would consist of a two-step Tikhonov-FP approach. The FP approach provides high resolution if the parameterized function describing the profile is on the one hand sufficiently constrained so that non-physical point-to-point variations are avoided, but on the other hand sufficiently flexible. As it is not always clear what the optimal parameterization should actually be, it would be helpful to

have unbiased additional information available on the shape of the profile. The Tikhonov-method provides such information. For example, for the emission profile studied in Sec. III B, it strongly suggests that profile has the shape of a single broad peak located more close to the anode. Thereby, alternative solutions such as a double-peaked profile can be excluded. For the emission profile studied in Sec. III D, the results obtained from the Tikhonov method show quite clearly that the emission is confined to the region in between the two interfaces, thereby excluding (major) contributions due to emission elsewhere. The occurrence of such contributions can often not be excluded *a priori*, as that will depend on the effectiveness of the electron or hole blocking at the interfaces. A two-step approach, consisting of (i) a pre-analysis using the Tikhonov method in order to determine an appropriate parameterized fit function and (ii) application of the FP method, is therefore expected to provide in general an improvement of the resolution.

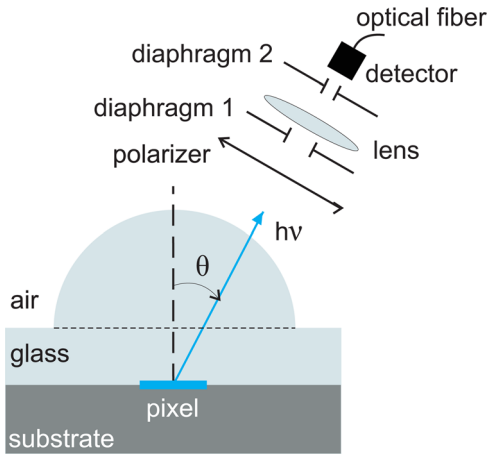

FIG. 6. (Color online) Schematic of the experimental set-up. Light emitted through the glass side of OLEDs is coupled into an optical fiber through a double-diaphragm system. The light collection system can rotate describing an angle θ.

ACKNOWLEDGMENTS

The authors thank H. Greiner for support when using the Lightex program and useful discussions, and Sumation Co., Ltd. for the supply of Lumation™ Blue Series polymers. This work forms part of the research program of the Dutch Polymer Institute (Project #518). The research has also received funding the European Community's Seventh Framework program under Grant Agreement No. 213708 (AEVIOM, contribution R.C.).

APPENDIX: EXPERIMENTAL PRECISION AND ACCURACY

In this appendix, we discuss the systematic and random errors which can occur in the measurement of the electroluminescence spectra. They determine the ultimate resolution of the light-emitting profile reconstruction methods discussed. For this purpose, we have carried out a study of the measurement uncertainties for the case of a blue-emitting polymer-based OLED. The layer stack is, from anode to cathode: glass (1 mm)/ITO (125 nm)/PEDOT:PSS (100 nm)/PF-TAA (100 nm)/barium (5 nm)/aluminum (100 nm), where the light-emission takes place in a polyfluorene-7.5 wt.% triarylamine copolymer (PF-TAA) with a structure which is presented in Ref. 20. The refractive index functions of the layers included are also given in Ref. 20. We regard the results of the analysis as representative and also applicable to (for example) small-molecule based white multilayer OLEDs.

The angular-dependent emission spectra have been measured using a Melcher Autronic DMS system. A schematic drawing of the experimental set-up is shown in Fig. 6. We measure the radiance emitted by a pixel via a light collection system composed of two diaphragms and a lens which focuses the collected light on the entrance of an optical fiber, mounted on a mechanical arm which can rotate around the pixel, describing an angle θ. A polarizer is mounted between the sample and the first diaphragm, which fixes the opening angle to 2°. By changing the size of the second diaphragm, closer to the fiber, one can change the size of the observed spot on the sample. The distance from the OLED pixel to the objective lens is approximately 15 cm. A glass hemisphere (radius 4 cm) is mounted on top of the glass substrate (1 mm), separated by an index matching fluid (dashed line in the figure). It can be demonstrated that such a large value for the hemisphere radius, much larger than the pixel size which is at most 1 mm, prevents curvature distortion effects on the collected angular-dependent spectra.

The use of small pixels greatly facilitates the alignment of the sphere with respect to the center of the observed spot. However, the finite pixel size can also be a cause of systematic errors, viz., when the measurement conditions are such that the area as seen by the detector is determined in part by the finite size of the OLED. Three measurement regimes can be distinguished, depending on the ratio between the observation spot diameter d (in glass and at $\theta = 0°$) and the size l of the squared OLED pixel, $r \equiv d/l$. In order to investigate the occurrence of systematic errors, the three regimes have been studied by carrying out measurements without and with the glass hemisphere. The pixel size was $l = 1$ mm, and the spot diameter in air was equal to 0.2, 1.0, and 3.0 mm, i.e., $d = 0.13$, 0.67, and 2.0 mm, using $n = 1.5$ as the refractive index of glass. For the cases where $r = 0.13$ and 2.0 (i.e., $d = 0.13$ and 2.0 mm) the spot size is for all emission angles smaller and larger than the pixel size, respectively, whereas for the intermediate $r = 0.67$ case the spot as seen without the hemisphere just falls within the pixel for normal emission but becomes at finite emission angles immediately larger than the pixel size. Figure 7 (symbols) shows the measured ratio η between the "emission in air" (i.e., measured without a hemisphere), P_{air}, and the "emission in glass" (i.e., measured using a glass hemisphere), P_{glass}, for a selected wavelength and for the three measurement regimes mentioned above. The result was found to be wavelength-independent. The results are given as a function of the polar emission angle in glass. In the experiments without a hemisphere, the

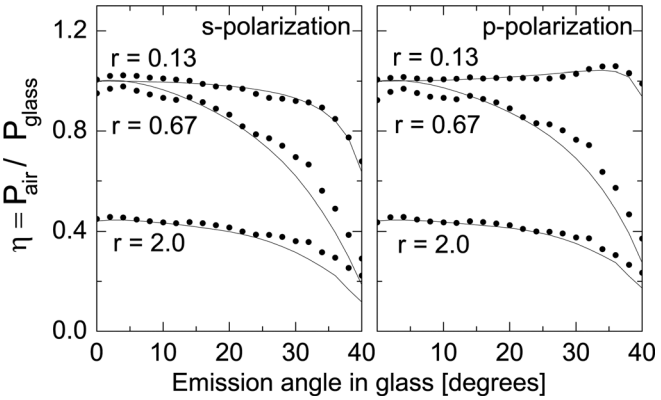

FIG. 7. Calculated (solid curve) and experimental (symbols) value of the ratio η between the power emitted in air and the power emitted in glass, as a function of the emission angle in glass, for *s*-polarized and *p*-polarized light, as indicated on the figure. Three possible measurement conditions are investigated, described by the ratio $r = d/l$ between the diameter of the observation spot, d, and the size of the squared pixel, l.

highest value, 38.8°, gives rise to emission at 70° in air. In the figure, these intensities are compared to the intensities measured with a hemisphere in the range (in glass and in air) up to 38.8°. For the three measurement regimes, a different angular- and polarization-dependence is expected for η. This is confirmed by the results of emission calculations including the angular dependent Fresnel refraction and reflection at the glass-air interface and including for the $r = 0.13$ and 0.67 cases the finite pixel size effect by means of a ray-tracing approach (solid curves).

The theoretical results at 0° can be understood as follows. After transmission from the glass substrate to the air, the emission solid angle increases by a factor n^2. On the other hand, the observed spot area in the glass is reduced by a factor n^2 if the spot is much smaller than the pixel size used. Overall, this leads to a ratio $\eta = 1$, in agreement with the observed $r = 0.13$ result. When the spot size in glass is larger than the pixel size, the ratio η reflects purely the solid angle increment. Its effect is not compensated by a spot size increase, so that $\eta = 1/n^2 \simeq 0.44$, in agreement with the observed $r = 2.0$ result. For an intermediate value of the spot radius, η is at 0° found to be slightly smaller than predicted. We interpret this as a result of a somewhat decreased emission intensity from the region close to the pixel boundary. This can affect the intensity observed in air, as the 1 mm spot radius is then equal to the size of the squared pixel, but not the intensity observed in the case of emission in glass, as the observed spot size in glass is then only 0.67 mm, well below the pixel size.

For higher emission angles, the calculations accurately describe the small-spot case ($r = 0.13$), whereas for the large-spot case ($r = 2.0$) the experimental curves deviate at high angles (larger than $\sim 30°$) somewhat from the calculated curves. We will discuss two factors which play a role, both related to the finite (1 mm) thickness of the glass substrate: multiple reflection in the glass substrate and parallax alignment errors. Multiple reflection in the glass substrate leads to a "light recycling effect:" in the case of a large spot size light which is reflected at the glass/air interface and subsequently to a point outside the OLED pixel can finally still be collected. It should be noted that the OLED pixel size is determined by the size of the patterned ITO anode, whereas the emissive layer and the reflecting cathode are not patterned. The effect is expected to increase with increasing angle, consistent with the observations. In the ultimate limit (multiple reflections with large reflection coefficients), finally all light would be collected, irrespective of the polarization. This may explain why for the large-spot case at high angles the experimental curves are for both polarizations more similar than as calculated (without taking multiple reflection effects into account). The influence of multiple reflections is expected to be less in the small-spot case, consistent with the results shown in the figure.

Second, we consider possible systematic errors due to a parallax error in the alignment of the spot center with respect to the pixel center. As a result of the finite thickness of the glass substrate, the actual position of the spot center varies slightly with respect to the OLED pixel center with increasing emission angle. This parallax error can be minimized as follows. First, perfect alignment and focus (height adjustment) is created for $\theta = 0°$. Subsequently, perfect spot angle alignment is realized at the highest polar angle included by a slight height adjustment (while keeping the lateral alignment the same). Although this introduces a small defocus, it strongly reduces the spot center alignment error. We have experimentally and theoretically investigated the remaining effect as a function of the glass substrate thickness. The effect is absent in the large spot-size case. For the small spot-size case it becomes larger with increasing glass thickness. However, for all cases shown in Fig. 7 (1 mm substrate) the remaining effect is found to be negligible. In conclusion, in order to minimize systematic errors the glass substrate thickness should be taken sufficiently small. For a small spot-size this will reduce remaining parallax errors, whereas for a large spot size this will reduce errors related to multiple reflection.

In general, systematic errors may also be introduced by errors in the wavelength dependent complex refractive index functions of the materials present in the OLED stack. To a certain extent it is possible to detect such errors by minimizing the χ^2 function with respect to the thickness of the layer for which the refractive index is uncertain. We furthermore stress that although such errors would lead to an error in the absolute position of the light-emission profile, the resolution with which various other relevant predictions can be made, such a shift in the emission profile with the OLED driving voltage, is not or only weakly affected.

In order to determine random errors affecting the accuracy of the measurements, we have investigated the reproducibility of the experimental spectra obtained for the same OLED as studied above. The spread between nominally identical measurements is found to be slightly angle, wavelength and polarization dependent. The error is smaller for higher emission intensities. At low voltages the ultimate measurement accuracy is determined by the occurrence of slow drift in the emission intensities during the large total measurement times needed, which limits the total data accumulation time to in practice a few hours. The highest errors are then obtained in the low-intensity parts of the spectrum and at large angles. For the blue OLEDs studied at a low brightness (4 cd/m^2 at 0°) the highest error is in the range 2%–4% (defined here and

below as the standard deviation of the intensity distribution), as obtained for *p*-polarized light in the 550–600 nm wavelength range and in the 55°–70° polar angle range. Outside this angle and wavelength range, the error is well below 1.5%. Also at high voltages, the ultimate measurement accuracy is determined by the drift, which is now much faster due to the larger effect of self-heating. However, much shorter measurement times are then feasible due to the larger signal. A conservative estimate of the resulting random intensity error is 2%. We use this error in our analysis of resolution limits of the emission profile for the blue OLEDs in Sec. III B. In the other case-studies presented in Sec. III we assume, even more conservatively, 5% random errors.

[1]N. Anscombe and O. Graydon (eds.), Nat. Photon. Technology Focus **3**, 8 (2009).
[2]S. Reineke, F. Lindner, G. Schwartz, N. Seidler, K. Walzer, B. Lüssem, and K. Leo, Nature **459**, 234 (2009).
[3]K. H. Kuma, Y. Jinde, M. Kawamura, H. Yamamoto, T. Arakane, K. Fukuoka, and C. Hosokawa, Society for Information Display (SID) Symposium Digest of Technical Papers **38**, 1504 (2007).
[4]S. L. M. van Mensfoort, J. Billen, M. Carvelli, S. I. E. Vulto, R. A. J. Janssen, and R. Coehoorn, J. Appl. Phys. **109**, 064502 (2011).
[5]J. J. M. van der Holst, F. W. A. van Oost, R. Coehoorn, and P. A. Bobbert, Phys. Rev. B **80**, 235202 (2009).
[6]M. Kuik, H. T. Nicolai, M. Lenes, G.-J. A. H. Wetzelaer, M. Lu, and P. W. M. Blom, Appl. Phys. Lett. **98**, 093301 (2011).
[7]G.-J. A. H. Wetzelaer, M. Kuik, H. T. Nicolai, and P. W. M. Blom, Phys. Rev. B **83**, 165204 (2011).
[8]C. W. Tang, S. A. VanSlyke, and C. H. Chen, J. Appl. Phys. **65**, 3610 (1989).
[9]M.-H. Lu and J. C. Sturm, J. Appl. Phys. **91**, 595 (2002).
[10]W. M. V. Wan, N. C. Greenham, and R. H. Friend, J. Appl. Phys. **87**, 2542 (2000).
[11]J.-S. Kim, P. K. H. Ho, N. C. Greenham, and R. H. Friend, J. Appl. Phys. **88**, 1073 (2000).
[12]T. Granlund, L. A. A. Pettersson, and O. Inganäs, J. Appl. Phys. **89**, 5897 (2001).
[13]J. M. Leger, S. A. Carter, B. Ruhstaller, H.-G. Nothofer, U. Sherf, H. Tillman, and H.-H. Hörhold, Phys. Rev. B **68**, 054209 (2003).
[14]H. Kuma, H. Tokairin, K. Fukuoka, and C. Hosokawa, Society for Information Display (SID) Symposium Digest of Technical Papers **36**, 1276 (2005).
[15]M. Roberts, Proc. of OEC-06 1 (2006).
[16]B. Ruhstaller, T. Flatz, M. Moos, G. Sartoris, M. Kiy, T. Beierlein, R. Kern, C. Winnewisser, R. Pretot, N. Chebotareva, and P. van der Schaaf, SID Symposium Digest of Technical Papers **38**, 1686 (2007).
[17]M. C. Gather, M. Flämmich, N. Danz, D. Michaelis, and K. Meerholz, Appl. Phys. Lett. **94**, 263301 (2009).
[18]B. Perucco, N. A. Reinke, D. Rezzonico, M. Moos, and B. Ruhstaller, Opt. Expr. **18**, A246 (2010).
[19]Software SETFOS by Fluxim AG, Switzerland, www.fluxim.com
[20]S. L. M. van Mensfoort, M. Carvelli, M. Megens, H. Greiner, D. Wehenkel, M. Bartyzel, R. A. J. Janssen, and R. Coehoorn, Nat. Photon. **4**, 329 (2010).
[21]A. N. Tikhonov and V. Y. Arsenin, *Solutions of Ill-Posed Problems* (Winston, Washington, DC, 1977).
[22]R. C. Aster, B. Borchers, C. Thurber, *Parameter Estimation and Inverse Problems* (Academic, New York, 2004).
[23]P. C. Hansen, *Discrete Inverse Problems* (SIAM, Philadelphia, 2010).
[24]H. Greiner and O. J. F. Martin, Proc. of SPIE **5214**, 249 (2004).
[25]Matlab Optimization Toolbox, The MathWorks, Inc.
[26]M. Carvelli, R. A. J. Janssen, and R. Coehoorn, Phys. Rev. B **83**, 075203 (2011).
[27]S. Harkema, R. A. H. J. Kicken, B. M. W. Langeveld-Voss, S. L. M. van Mensfoort, M. M. de Kok, and R. Coehoorn, Organ. Electr. **11**, 755 (2010).